Microfluid Nanofluid (2010) 8:619–629
DOI 10.1007/s10404-009-0494-6

RESEARCH PAPER

Compressible flows through micro-channels with sharp edged turns and bifurcations

Amir D. Gat · Itzchak Frankel · Daniel Weihs

Received: 10 May 2009 / Accepted: 3 August 2009 / Published online: 20 August 2009

Abstract Bends and bifurcations connecting straight channels are common features in micro-channel networks. We apply our recently extended Hele-Shaw asymptotic scheme to study the viscous compressible gas flow through a shallow bend (whose depth is small relative to all other characteristic dimensions). By the use of analytic-function theory, we obtain closed-form solutions for arbitrary values of the turn angle and the ratio between the upstream- and downstream- channel widths, respectively. The viscous resistance is thereby evaluated in terms of the geometrical parameters characterizing the bend. The linearity of the problem in terms of an appropriately defined quadratic form of the pressure allows us to briefly consider the role of bifurcations in the viscous resistance of tree-like micro-channel networks.

Keywords Micro-channel bends · Tree-like networks · Micro-flows · Viscous compressible flow

1 Introduction

Micro-fluidics play a central role in numerous micro-system applications (e.g., the cooling of micro-electronic systems, micro fuel cells, and flow control etc., Ho and Tai 1996, 1998; Gad-el-Hak 1999, 2002). In this contribution, we focus on the fluid motions through micro-channel bends and bifurcations which are common features in many micro-fluidic systems (Bejan and Lorente 2006; Xiong and Chung 2007). Much interest focuses on tree-like networks comprising a hierarchy of bifurcations (Zimaparov et al. 2006; Durand 2006; Ding and Yamazaki 2007; Barber and Emerson 2008), since experimental and theoretical evidence indicate that such biologically inspired networks provide higher effectiveness (in terms of mass flow rate in pressure driven micro-flows) than the corresponding systems employing parallel-channel configurations (Ghodoossi 2004; Chen and Cheng 2005). Bends and bifurcations can have a significant contribution to the total pressure-drop through the networks, and their study is accordingly essential to the optimization of such systems (Alharbi et al. 2003; Senn and Poulikakos 2004; Wechsatol et al. 2006).

Typical of many micro-fluidic devices produced by current micro-fabrication technology, is that the flow takes place within the narrow (≈ 1 μm) gap between parallel planes. Furthermore, these configurations are often shallow in the sense that the gap width is much smaller than all other characteristic dimensions (e.g., channel widths which are ≈ 10–10^2 μm, Arkilic et al. 1997; Lee et al. 2001; Zohar et al. 2002).

Owing to these geometrical features the resulting flows are nearly isothermal (cf. Gat et al. 2008 and references cited therein), and fluid-inertial effects are usually negligible, the dominant balance being between the viscous resistance and the pressure-drop. The latter is accompanied by significant fluid-density variations regardless of the small Mach numbers involved ('low-Mach compressibility'). Furthermore, for gaseous micro-flows under standard atmospheric conditions the Knudsen number (i.e., the ratio between the molecular mean-free path and the gap width) is typically $Kn \approx 10^{-2}$–10^{-1}. Thus, these flows are subject to weak rarefaction effects (Cercignani 2000).

Lee et al. (2001) have carried out an experimental investigation of gas flows through various types of turns in shallow micro-channels. In the absence of more suitable

A. D. Gat (✉) · I. Frankel · D. Weihs
Faculty of Aerospace Engineering, Technion—Israel Institute of Technology, Technion City, Haifa 32000, Israel
e-mail: gat@tx.technion.ac.il

analyses, they (as well as others, Yu et al. 2005; Agrawal et al. 2005) have interpreted and correlated their results by making reference to the analysis of Arkilic et al. (1997) which, however, strictly applies only to straight and uniform shallow micro-channels. The principle goal of the present contribution is thus to analyze the compressible flow through a turn of arbitrary angle, or a symmetric bifurcation, joining straight micro-channels (for a general ratio of their respective widths). The resulting analytic approximation will then be applied to discuss the effects of symmetric bifurcations on the pressure losses in the flows through tree-like micro-channel networks.

The combination of a narrow-gap shallow geometric configuration and small Reynolds number suggests that the above goal may be achieved through the application of a Hele-Shaw approximation. The corresponding classic problem formulation (cf. Batchelor 1967) is concerned with incompressible flows and is incapable of satisfying the requisite boundary conditions on the tangential fluid velocity at the lateral walls. Gat et al. (2008) have extended the theory to viscous gas flows still without properly accounting for the boundary conditions at the side walls. Comparison of their approximate analytic results with finite-element simulation has, however, demonstrated that the failure to satisfy these conditions restricts the practical value of the resulting approximation to very shallow configurations. In a recent contribution Gat et al. (2009) have extended the Hele-Shaw scheme to incorporate the side-wall boundary conditions. This extended asymptotic scheme will here be applied to the analysis of viscous gas flows through shallow turns and symmetric bifurcations.

In the next section, we define the geometric configuration of the bend, formulate the problem and outline the asymptotic scheme of Gat et al. Analytic solutions are then obtained in Sect. 3 through application of this scheme in conjunction with conformal mapping. These solutions are subsequently utilized to calculate the pressure-head loss or the reduction of mass flow rate through the shallow bend. In Sect. 4, we discuss the validation of the present analysis by comparison with numerical simulations, the effects of the geometrical parameters of the turn on the pressure-head losses and briefly consider the effects of bifurcations on the flow through tree-like micro-channel networks. Concluding remarks are made in Sect. 5 and explicit closed-form expressions for particular values of the turn angle are tabulated in the appendix.

2 Analysis

2.1 Formulation of the problem

We consider the viscous compressible flow of a perfect gas through the bend schematically depicted in Fig. 1. The bend of uniform depth $2H$ connects two straight and uniform channels forming an angle α. The lateral dimensions of the downstream and upstream channels are D and dD, respectively and the corresponding longitudinal dimensions are L_1 and L_2, respectively. For given dimensions D, H, L_1, and L_2 all possible configurations are obtainable through varying the values of α and the dimensionless parameter d. We select the Cartesian frame whose origin is at the inner corner of the bend. The x and y axes lie at the bend midplane (x pointing in the upstream direction) and the z axis is perpendicular thereto. In subsequent derivation the dimensionless (x, y) coordinates are scaled by D and the z coordinate by H. For the normalization of fluid velocity, we select the scale $U = p_0H^2/\mu D$, wherein p_0 is an appropriate reference value of the pressure-drop and μ denotes the gas viscosity, thus reflecting the above-mentioned dominant balance between pressure-drop and viscous resistance. The components $\mathbf{u}_{\|} = (\mathrm{u}, \mathrm{v})$ of the fluid velocity vector in the (x, y) plane are normalized by U and the corresponding z component of the velocity, w, is scaled by UH/D.

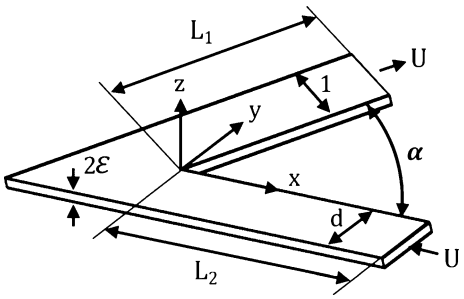

Fig. 1 Definition of the geometrical parameters of the bend and the Cartesian coordinates. All dimensions are normalized by D, the width of the downstream channel

As mentioned in the Introduction, gas flows through micro-configurations taking place under standard atmospheric conditions are characterized by $Kn \approx 10^{-2}$–10^{-1} corresponding to weak rarefaction effects. We therefore consider the problem through use of a continuum slip-flow model (see also Sect. 5). Within the framework of this model, the isothermal motion of the gas is still governed by the continuity and Navier–Stokes equations. However, the no-slip conditions at solid walls are here replaced by first-order Navier-type slip conditions imposed on the fluid velocity tangential to the wall (Cercignani 2000). Extensive theoretical and experimental (Arkilic et al. 1997; Ho and Tai 1998; Gad-el-Hak 1999; Sharipov 1999; Zohar et al. 2002) evidence support the use of these simplified continuum models to account for weak rarefaction effects.

For a shallow configuration, we define the pair of small parameters

$$\varepsilon = \frac{H}{D} \ll 1 \tag{1}$$

(for $d < 1$, we actually require that $\varepsilon/d \ll 1$, cf. Fig. 1) and the reduced Reynolds number $\varepsilon\mathrm{Re} \ll 1$, where

$$\mathrm{Re} = \frac{\rho_0 UH}{\mu}. \tag{2}$$

In Eq. 2 ρ_0 is the gas density for p_0 and the (uniform) reference temperature. Following the derivation by Gat et al. (2008), we find that, to leading order in the small parameters ε and $\varepsilon\mathrm{Re}$, the viscous gas motion through the shallow bend is governed by the equations

$$\frac{\partial}{\partial x}(\rho u) + \frac{\partial}{\partial y}(\rho v) + \frac{\partial}{\partial z}(\rho w) = 0, \tag{3}$$

$$\frac{\partial p}{\partial x} = \frac{\partial^2 u}{\partial z^2} + O\left(\varepsilon\mathrm{Re}, \varepsilon^2\right), \tag{4}$$

$$\frac{\partial p}{\partial y} = \frac{\partial^2 v}{\partial z^2} + O\left(\varepsilon\mathrm{Re}, \varepsilon^2\right), \tag{5}$$

$$\frac{\partial p}{\partial z} = O\left(\varepsilon^3\mathrm{Re}, \varepsilon^2\right), \tag{6}$$

and

$$p = \rho, \tag{7}$$

representing the dimensionless equation of continuity, the Cartesian components of the equation of motion and the equation of state of a perfect gas, respectively. In Eqs. 3–7, the coordinates and velocity components are normalized as stated above; pressures and densities are scaled by p_0 and ρ_0, respectively. The above equations are supplemented by the impermeability condition

$$\hat{\mathbf{n}} \cdot \mathbf{u} = 0 \tag{8}$$

on the bend walls, the first-order slip condition (Sone 2002)

$$\mathbf{u}_{||} = \mp\sigma Kn_0 p \frac{\partial \mathbf{u}_{||}}{\partial z} \quad \text{at } z = \pm 1 \tag{9}$$

(top and bottom of the channel, respectively), no-slip conditions on lateral walls (neglecting $O(\varepsilon Kn)$ contributions for $Kn \ll 1$, cf. Gat et al. 2009) and appropriate conditions imposed on the velocities or pressures at the entrance and exit sections of the bend. In Eq. 9 Kn_0 denotes the Knudsen number at the reference pressure p_0 and σ is the viscous-slip coefficient representing the interaction between gas molecules and the solid walls. We, here, employ the value $\sigma = 1.1466$ obtained by Albertoni et al. (1963) (see also Sharipov 1999; Aubert and Colin 2001; Ewart et al. 2007). The above-formulated problem is addressed through application of the recently extended Hele-Shaw scheme (Gat et al. 2009) which is outlined next.

2.2 Recapitulation of the extended Hele-Shaw scheme

Following Gat et al. (2009), we integrate Eqs. 3–6 across the channel depth while making use of Eqs. 7 and 9 to express the velocity field in terms of the pressure as

$$\mathbf{u}_{||} = -\left[\frac{1}{2}\left(1 - z^2\right) + \frac{\sigma Kn_0}{p}\right]\nabla_{||} p \tag{10}$$

and

$$w = \frac{z}{p}\nabla_{||}^2\left[\frac{1}{4}\left(1 - \frac{z^2}{3}\right)p^2 + \sigma Kn_0 p\right] \tag{11}$$

where $\nabla_{||} = \mathbf{i}\,\partial/\partial x + \mathbf{j}\,\partial/\partial y$ is the planar part of the gradient operator. Defining the quadratic form[1]

$$G = \frac{1}{6}p^2 + \sigma Kn_0 p \tag{12}$$

Equations 7 and 10 yield

$$\int_0^1 \rho \mathbf{u}_{||} dz = -\nabla_{||} G. \tag{13}$$

Thus, G may be considered as scalar potential of the mass-flux-density vector (per unit width) in the two-dimensional planform domain defined by the intersection of the channel mid-plane with its side walls. Furthermore, integration of Eq. 3 across the channel depth in conjunction with Eq. 8 and Eqs. 10–12 yields

$$\nabla_{||}^2 G = 0, \tag{14}$$

i.e., G is harmonic within the two-dimensional planform domain.

Typical of the leading order Hele-Shaw approximation is that the no-slip (or Navier slip) conditions at the side walls of the configuration cannot be satisfied. In order to overcome this limitation, Gat et al. (2009) have extended the Hele-Shaw scheme for small Reynolds and Knudsen numbers. To begin with G is expanded as

$$G(x, y) \sim G_0(x, y) + \varepsilon\bar{c} G_1(x, y) + O\left(\varepsilon^2, \varepsilon\mathrm{Re}, \varepsilon Kn\right) \tag{15}$$

where similarly to G both G_0 and G_1 are harmonic within the two-dimensional configuration planform domain. By Eq. 8 G_0 satisfies

$$\frac{\partial G_0}{\partial n} = 0 \text{ on } \Gamma, \tag{16}$$

where Γ is the part of the planform boundary formed by the channel side walls (thus excluding the part of the boundary

[1] For a uniform incompressible fluid ($\rho = $ const.) the classical Hele-Shaw model (Batchelor 1967) is recovered by defining instead $G = p/3$.

corresponding to the channel entrance and exit sections); $\partial/\partial n$ denotes differentiation along the normal to Γ directed into the fluid domain. The statement of the problem governing G_0 (and G_1 as well) is completed by imposing appropriate Dirichlet or Neumann conditions at the entrance and exit sections (according as the pressures of fluid mass flow rate densities are specified there, see also in the next section).

In order to satisfy the appropriate conditions on the tangential velocity at the side walls, an inner solution is constructed for the fluid velocity in the immediate $O(\varepsilon)$ vicinity of the lateral walls. The leading order of this field is uniquely determined through an asymptotic matching to G_0 in their common domain of validity. From the inner solution thus obtained we calculated $\bar{c}$ (≈ 0.63 for a rectangular channel cross section; see Gat et al. 2009 for values corresponding to non-rectangular cross sections). An asymptotic matching of the inner leading order solution to the $O(\varepsilon)$ outer correction yields for G_1 the condition

$$\frac{\partial G_1}{\partial n} = \frac{\partial^2 G_0}{\partial s^2} \text{ on } \Gamma, \tag{17}$$

where $\partial/\partial s$ denotes differentiation along Γ. This, together with the appropriate conditions imposed at the entrance and exit sections (see above as well as in Sect. 3) uniquely determine the harmonic function G_1.

It is useful to note that the presentation (Eq. 15) is useful in that it separates the effects of ε and the cross-sectional geometry from those of the planform configuration which are embodied in G_0 and G_1. The entire viscous compressible flow problem is thereby reduced to a pair of Dirichlet–Neumann problems. Furthermore, for a given planform configuration these problem need to be solved only once. In the next section, we demonstrate how the calculation of G_0 and G_1 serve to determine (correct to $O(\varepsilon)$) the viscous resistance of the shallow bend configuration.

3 The viscous resistance of the shallow bend configuration

3.1 Calculation of G

We begin by considering the problem when the mass flow rate (rather than the entrance and exit pressures) is specified. The problem is further simplified by replacing the actual finite configuration (depicted in Fig. 1) by a bend joining a pair of semi-infinite straight and uniform channels. In this case far upstream and downstream the flow becomes parallel and uniform across the channel width (with the exception of the $O(\varepsilon)$ neighborhood of the lateral walls). By use of the relation (Eq. 13) it is readily verified that for a unit mass flow rate

$$\frac{\partial G_0}{\partial n} = -1,\ -1/d \quad \text{and} \quad \frac{\partial G_1}{\partial n} = -2,\ -2/d^2 \tag{18}$$

far downstream and upstream, respectively. In order to obtain G_0, we consider it as the real part of the analytic-function $F_0(t) = G_0(x,\ y) + iQ_0(x,\ y)$ of the complex variable $t = x + iy$ and map the planform domain in the physical t-plane onto the upper half of the auxiliary $\zeta = \xi + i\eta$ plane (see Fig. 2). This mapping is accomplished through application of the Schwarz–Christoffel transformation

$$\frac{dt}{d\zeta} = K\frac{\zeta^{1-\frac{\alpha}{\pi}}}{(\zeta - a)(\zeta + 1)}, \tag{19}$$

where the parameters K and a are evaluated from the requirements that the outlet and inlet dimensionless widths are unity and d, respectively. We thus obtain

$$t(\zeta) = d^{\frac{\pi}{\pi-\alpha}}\frac{\zeta^{\frac{\alpha}{\pi}-2}e^{i(\alpha-\pi)}}{\alpha - 2\pi}\left[\begin{array}{c} d^{\frac{-\pi}{\pi-\alpha}}F_1\left(1, 2-\frac{\alpha}{\pi}, 3-\frac{\alpha}{\pi}, d^{\frac{-\pi}{\pi-\alpha}}\zeta\right) \\ +F_1\left(1, 2-\frac{\alpha}{\pi}, 3-\frac{\alpha}{\pi}, -\zeta\right)\end{array}\right], \tag{20}$$

where

$$F_1(q, s_1, r, z) = \frac{\Gamma(r)}{\Gamma(s_1)\Gamma(r-s_1)}\int_0^1 \frac{\zeta^{s_1-1}(1-t_1)^{r-s_1-1}}{(1-t_1 z)^q}dt_1 \tag{21}$$

denotes the Gauss hyper-geometric function (Abramowitz and Stegun 1964). The function F_0 is readily obtained in the ζ-plane as a source-type logarithmic function. Once G_0 has been evaluated G_1 satisfying Eq. 17 is expressed through the use of Green's function for the Neumann problem in the upper half ζ-plane (cf. Polyanin 2002) to yield eventually

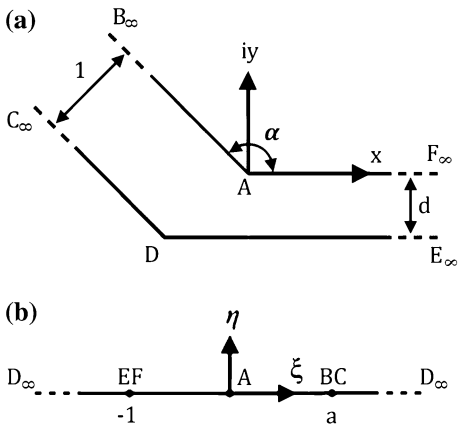

Fig. 2 The domain of the Neumann problem governing G: The physical t-plane within the channel planform (**a**) and the auxiliary ζ-plane (**b**)

$$G[t(\zeta)]=\frac{1}{\pi}\left[\ln\left(\left|1-\zeta d^{-\frac{\pi}{\pi-\alpha}}\right|\right)(1+2\varepsilon\bar{c})-\ln(|1+\zeta|)\left(1+2\varepsilon\frac{\bar{c}}{d}\right)\right] -\frac{\bar{c}\varepsilon}{2\pi}\int_{-\infty}^{\infty}\left[\frac{\partial}{\partial\beta}\left(\frac{1}{|t'(\beta)|}\frac{\partial}{\partial\beta}\ln\left(\frac{1-\beta d^{-\frac{\pi}{\pi-\alpha}}}{1+\beta}\right)\right)\right] \ln\left[(\xi-\beta)^2+\eta^2\right]d\beta, \tag{22}$$

where a prime denotes differentiation with respect to the argument. Thus, for a given channel planform, i.e., prescribed values of α and d, the complete solution for G is given by Eq. 22 together with Eq. 20. For the particular values of $\alpha = \pi/4$, $\pi/2$, and $3\pi/4$ the transformation t(ζ) may be expressed in terms of elementary functions (inverse tangent and inverse hyperbolic tangent, see the Appendix).

3.2 Pressure-head loss associated with the turn

Owing to the nonlinear streamwise variation of the pressure (Arkilic et al. 1997), we focus the discussion of compressible flows on the variation of the quadratic form G. Thus, to quantify the losses associated with the bend, we compare the above calculated G to that corresponding to a unit dimensionless mass flow rate through straight and uniform channels. In such channels, it is readily established that G is uniform across the cross section and varies linearly in the streamwise direction. To begin with, we consider the function G_U corresponding to the upstream uniform channel whose cross section is identical to that of the entrance section (EF in Fig. 2). Selecting $G_U = 0$ at the origin we obtain

$$G_U=\left(1+2\varepsilon\frac{\bar{c}}{d}\right)\frac{x}{d}=\left(1+2\varepsilon\frac{\bar{c}}{d}\right)\Re\left[\frac{t(\zeta)}{d}\right], \tag{23}$$

where $\Re[\cdot]$ denotes the real part of the complex-valued expression. From the far-field condition (Eq. 18) it is clear that, for a given mass flow rate, the difference $G - G_U$ approaches a constant limit when $x \to \infty$. Making use of the coordinate definitions in the physical t-plane and auxiliary ζ-planes together with Eqs. 20 and 22, we may express this limit through

$$\Delta^u(\alpha,d,\varepsilon)=\lim_{\zeta\to-1}\{G[t(\zeta)]-G_U(\zeta)\}=\Delta_0^u+\varepsilon\bar{c}\Delta_1^u. \tag{24}$$

Here, similar to Eq. 15 for G, it is useful to present Δ^u in a manner which separates the effects of the cross-sectional geometry (represented by ε and $\bar{c}$) from those of the planform defined by α and d (see Fig. 2). The latter effects are embodied in Δ_0^u and Δ_1^u (whose explicit expressions are omitted). By the symmetry of the present problem, we readily obtain for the downstream part of the channel $\Delta^d(\alpha, d, \varepsilon) = \Delta^u(\alpha, 1/d, \varepsilon/d)$. The total difference between the actual drop of G through the entire (infinite) bend configuration and the sum of the corresponding drops through the pair of (semi-infinite) straight and uniform channels whose normalized widths are d and l respectively, is thus

$$\Delta(\alpha,d,\varepsilon)=\Delta^u(\alpha,d,\varepsilon)+\Delta^u\left(\alpha,\frac{1}{d},\frac{\varepsilon}{d}\right)=\Delta_0+\varepsilon\bar{c}\Delta_1. \tag{25}$$

Explicit expressions for Δ_0 and Δ_1 are readily obtained for $\alpha = \pi/4$, $\pi/2$ and $3\pi/4$ (see the Appendix).

The above analysis may be applied to estimate losses in finite-length configurations (see Fig. 1) when L_1 and L_2/d are sufficiently large and the flow becomes nearly uniform across the entrance and exit sections of the finite bend. Both the above analytic results and the numerical simulations carried out to produce the results presented in the next section demonstrate that this is already established for L_1, $L_2/d \geq 1$ (cf. Gat et al. 2008). The total G-difference between the entrance and exit section is thus

$$\Delta G = (1 + 2\varepsilon\bar{c})L_1 + \left(1 + 2\varepsilon\frac{\bar{c}}{d}\right)\frac{L_2}{d} + \Delta(\alpha,d,\varepsilon), \tag{26}$$

where the first two terms on the right-hand side represent the corresponding total difference for the same (unit) mass flow rate through a pair of finite segments (L_1 and L_2) of infinite straight uniform channels (of normalized widths l and d, respectively). We recognize that Δ is the present counterpart of the 'equivalent length' which is widely used (White 1986) in the literature on viscous incompressible flows through pipe systems to describe 'minor losses' associated with turns, valves, sudden expansions, or contractions etc., (i.e., the additional pressure-head relative to that required to drive the same mass flow rate through a comparable straight and uniform tube).

So far, we have considered the value of ΔG required to drive a unit dimensionless mass flow rate through the given shallow configuration. As demonstrated by Eq. 13, the mass-flux-density (per unit width of the channel) is proportional to $\nabla_{\|}G$. This, together with the linearity of the problem governing G, yield for the dimensionless mass flow rate (normalized by $2H^3p_0\rho_0/\mu$), through the finite-length bend (see Fig. 1)

$$\dot{m}=\frac{\Delta G}{L_1(1+2\varepsilon\bar{c})+\frac{L_2}{d}\left(1+\frac{2\varepsilon\bar{c}}{d}\right)+\Delta_0(\alpha,d)+\varepsilon\bar{c}\Delta_1(\alpha,d)}, \tag{27}$$

where ΔG is the total difference between the (assumed uniform) exit and entrance values of G. Thus $\Delta(\alpha, d, \varepsilon)$ also represents the reduction in the mass flow rate for a given value of ΔG.

3.2.1 A symmetric bifurcation

Within the framework of the present approximation, a symmetric bifurcation may be constructed by joining a pair of identical turns along the straight center streamline of the parent channel (e.g., the line DE line in Fig. 2a) whose dimensionless width now becomes $2d$. This replacement of a solid boundary by a reflection-symmetry line does not affect the calculation of G_0 (since it anyway satisfies a homogeneous Neumann condition there). Consequently, Δ_0 (whose calculation only depends upon G_0) is also the same for both the symmetric bifurcation and the corresponding bend. The corresponding calculation of G_1 needs to be modified since along the symmetry line (DE) the coefficient $\bar{c}$ vanishes. Furthermore, one needs to subtract the contribution of the line DE from the integral term in Eq. 22. The calculation of Δ_1 is accordingly modified (see Gat et al. 2009 for details and the Appendix for an illustration) and so is the expression Eq. 27 for the mass flow rate which now reads

$$\dot{m} = \frac{\Delta G}{L_1(1+\varepsilon\bar{c}) + \frac{L_2}{d}\left(1+\frac{2\varepsilon\bar{c}}{d}\right) + \Delta_0(\alpha,d) + \varepsilon\bar{c}\Delta_1(\alpha,d)}. \tag{28}$$

4 Results and discussion

The above approximate analysis assumes both ε and Re to be asymptotically small. We verify its prediction through a comparison with finite-element simulations by means of the COMSOL 3.4 software package. These simulations integrate the three-dimensional continuity, Navier–Stokes and energy equations governing viscous compressible flow without invoking any of the above geometric (shallowness) or physical (small Re) approximations. All the simulations have been carried out for the flow of air through 1 μm deep channels. A uniform temperature (293 K) has been assumed at the solid walls and across the entrance and exit sections. A standard atmospheric pressure has been prescribed at the exit section. The uniform entrance pressure has been adjusted so as to attain the specified value of Re at the exit. In order to simplify the validation, we have imposed in these simulations no-slip conditions at the walls (corresponding to selecting $Kn_0 = 0$ in the analysis). For the COMSOL simulations, we have selected a tetrahedral unstructured mesh including at least eight cells across the channel depth. This places a lower bound on the total number cells required for a given configuration imposing computational limitations on the smallest value of ε and the largest total length of the simulation domain which are practically realizable. The lengths of the channels comprising the bend have been selected so as to ensure fully developed flows at both entrance and exit sections (in agreement with the above analysis). For all the configurations employed, this condition has been satisfied provided that L_1, $L_2/d \geq 1$ (i.e., the length of the channel segments both downstream and upstream exceed their respective widths).

A global measure of the difference between the analysis and numerical simulations is provided in Figs. 3 and 4 by r_m, the ratio between the respective analytic and numerical calculations of the mass flow rate corresponding to a given combination of α, d and ε ($r_m = 1$ representing a perfect agreement). All cases presented concern rectangular cross sections ($\bar{c} \approx 0.63$) and equal dimensionless lengths (cf. Fig. 1) L_1, $L_2 = 1.5d$. (Since $d \geq 1$ in all cases presented, the above criterion for a fully developed flow at the entrance and exit sections is safely satisfied.)

Figure 3 examines the variation with ε of r_m for the typical (Zohar et al. 2002; Yu et al. 2005) Re = 0.1 at the exit section and the indicated combinations of α and d for a bend (a) and a symmetric bifurcation (b). In general, $r_m \geq 1$, i.e., the analytic prediction over-estimates the mass-flow rate. It is, however, remarkable that for the entire selection of geometric configurations, the deviation from the 'exact' numerical calculation is within $\approx$ 5% for $2\varepsilon \leq 0.4$ ($2\varepsilon = 1$ corresponding to a square cross section).

Figure 4 similarly examines the error associated with the neglect of fluid-inertial effects. To this end the figure presents the variation of r_m with exit section Reynolds number for the selection of bend configurations indicated. Up to Re $\approx$ 10 only rather mild variations of r_m are observed. It is interesting to note that in some cases (denoted by the squares) $r_m < 1$ and in others (the stars) the variation with Re in non-monotonical. The agreement demonstrated in Figs. 3 and 4 between the entirely independent numerical and analytic calculations of the mass-flow rate is very gratifying and substantiates the usefulness of our analytic scheme.

The effects of the geometric parameters α and d on the viscous resistance of turns and symmetric bifurcations are exclusively embodied in Δ_0 and Δ_1 which (for $\bar{c}$ given) determine the increase of ΔG required to drive a prescribed mass flow rate through the shallow configuration (Eq. 26) or, alternatively the reduction of mass flow rate for a given ΔG, (Eqs. 27, 28). Figure 5 presents the variation of Δ_0 with d for the indicated values of α. With the use of Eq. 25, one readily obtains the symmetry relation $\Delta_0(\alpha, d) = \Delta_0(\alpha, 1/d)$. It is therefore sufficient to describe the interval $0 \leq d \leq 1$. For all the cases presented Δ_0 attains minima at $d = 1$. Furthermore, these minima are diminishing with increasing α. With decreasing d, Δ_0 is increasing. Moreover, for d sufficiently small the order of the curves is reversed and larger values of Δ_0 are obtained for the larger α. While the former observation seems fairly obvious—larger α involves a

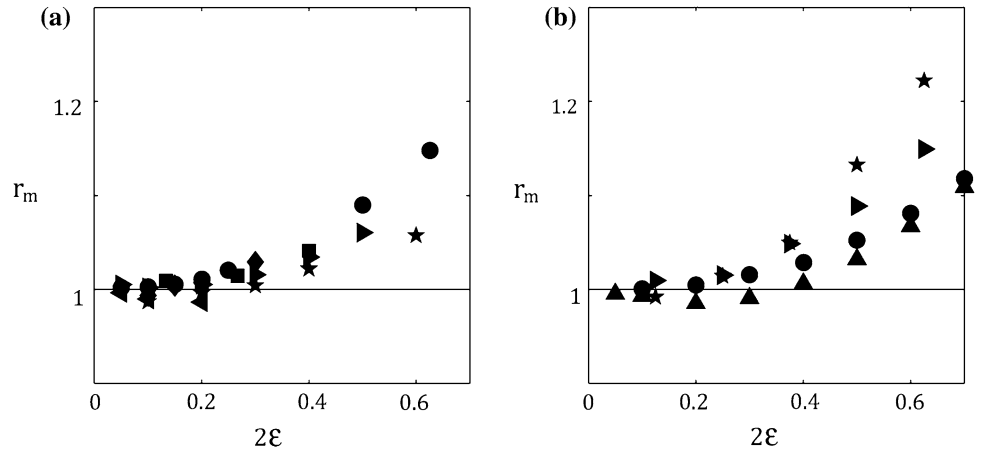

Fig. 3 The variation of r_m, the ratio of the respective analytic and numerically obtained mass flow rates, with the normalized channel height 2ε ($2\varepsilon = 1$ corresponding to a square cross section) for an exit Re = 0.1 for bend (**a**) and symmetric bifurcation (**b**) finite configurations with $L_1 = L_2 = 1.5d$ (see Fig. 1). Marked in the figure are the combinations (α, d) = ($\pi/2$, 1) (*circles*), ($\pi/2$, 4/3) (*squares*), ($3\pi/4$, 1) (*diamonds*), ($\pi/2$, 2) (*right-pointing triangles*), ($\pi/4$, 1) (*left-pointing triangles*), ($3\pi/4$, 2) (*stars*), and ($\pi/4$, 2) (*upward-pointing triangles*)

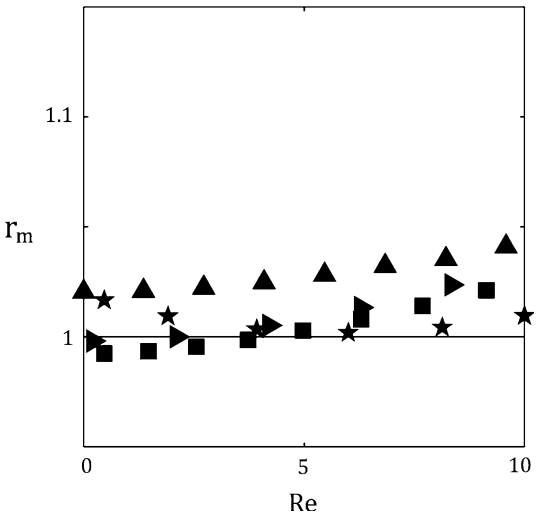

Fig. 4 The variation of r_m, the ratio of the respective analytic and numerically obtained mass-flow-rates with Re for finite bend configurations with $L_1 = L_2 = 1.5d$ (see Fig. 1). Marked in the figure are the combinations (α, d, 2ε) = ($\pi/2$, 1, 0.2) (*right-pointing triangles*), ($\pi/4$, 1, and 0.1) (*squares*), ($3\pi/4$, 2, and 0.2) (*stars*) and ($\pi/2$, 1, and 0.3) (*upward-pointing triangles*)

smaller deflection of flow direction (see Fig. 1)—the latter seems counterintuitive. In order to rationalize this reversal of trend it is useful to note that the configuration resistance is determined not only by the amount of rotation involved but also by the contraction or expansion involved in the transition between channels of unequal respective widths. The more abrupt this transition is the larger the latter contribution becomes. The above observed increase of Δ_0 with diminishing d (for fixed α) is thus associated with the transition between increasingly disparate channel widths. Furthermore, for a given $d \neq 1$, the 'effective' cross-sectional width in the transition region is diminishing with increasing α (the extreme case being $\alpha = \pi$ where the bend configuration turns into a sudden expansion or contraction). For $d \approx 1$ the former mechanism associated with the amount of rotation is dominant. With increasing $d > 1$ or decreasing $d < 1$, the latter influence prevails which brings about to the observed trend reversal.

Figure 6 presents the variation with d of Δ_1 for a turn (a) and a symmetric bifurcation (b) at the indicated values of α. In the part a of the figure it is sufficient to describe the variation over the interval $0 \leq d \leq 1$. For $d > 1$ Δ_1 may then be obtained through the use of the relation $\Delta_1(\alpha, d) = \Delta_1(\alpha, 1/d)/d$. In contrast with Δ_0, this relation does not imply a perfect symmetry about $d = 1$. Indeed, unlike Δ_0 in Fig. 5, Δ_1 here does not attain a minimum at $d = 1$. The quantity presented here, Δ_1, represents the $O(\varepsilon)$ correction associated with the retardation of fluid motion in the immediate vicinity of the channel side walls. With diminishing d the parameter

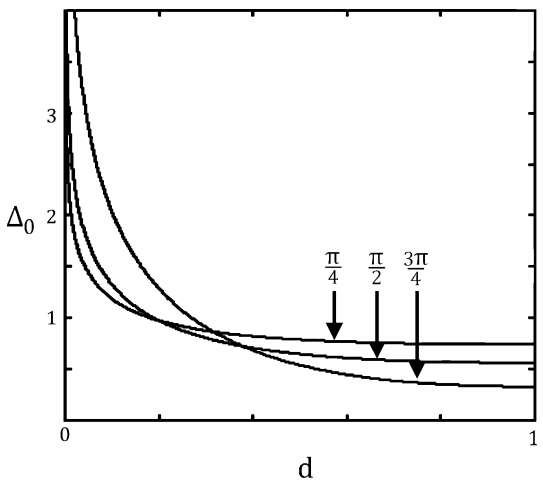

Fig. 5 Variation of Δ_0 with d for the indicated values of α

ε corresponding to the narrower channel is effectively increasing and so does Δ_1. Unlike the case of a bend, one cannot interchange the upstream and downstream sides in the calculation of Δ_1 for the bifurcation, hence Fig. 6b covers the interval $0 \leq d \leq 4$. Similar to that shown in Figs. 5 and 6a, Δ_1 is here diminishing with α for $d \approx 1$, which trend will eventually reverse for sufficiently small $d < 1$ and sufficiently large values of $d > 1$ (not explicitly presented here). In this context, note that, contrary to appearance, none of the curves presented in Fig. 6b has actually attained a constant asymptotic limit at $d = 4$).

4.1 Branching (tree-like) micro-channel networks

The above analysis of the flow through a single bend and a symmetric bifurcation will now be applied to examine the viscous resistance of tree-like micro-channel networks consisting of multiple symmetric bifurcations (see Fig. 7a). To this end, the entire system is represented as a combination of finite bifurcations (see Fig. 7b) and the flow

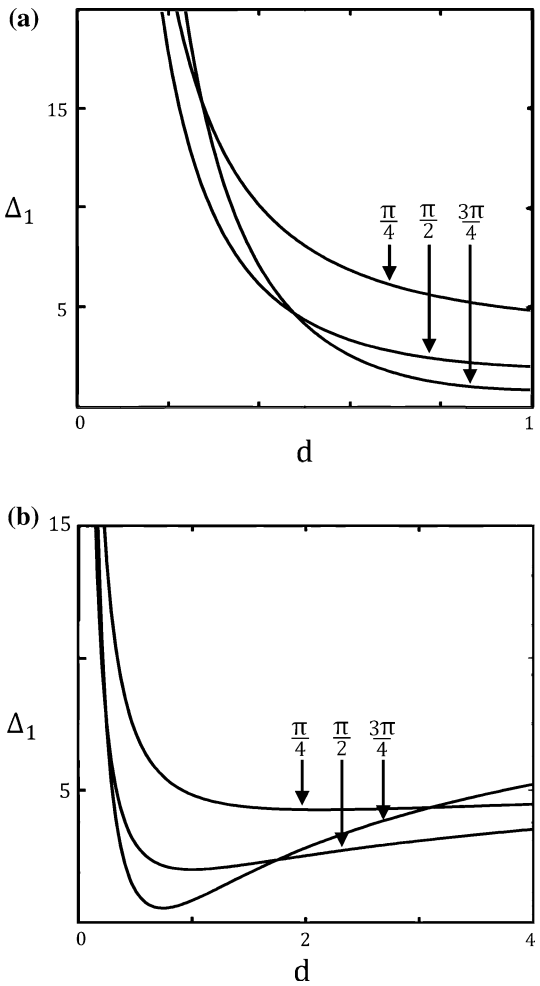

Fig. 6 Variation of Δ_1 with d for the indicated values of α for a bend (**a**) and a symmetric bifurcation (**b**)

through the network is described by putting together the separate segments making use of the analytic solution for a single bend obtained in the preceding sections. The nonlinear streamwise variation of the pressure in compressible flow apparently precludes this procedure of adding up contribution of the separate segments. This difficulty is, however, avoided through our present use of the quadratic form G which, for a given geometric configuration is linearly related to $\dot{m}$ through Eq. 28 (cf. also Gat et al. 2008, in particular their Fig. 6). An experimental evidence in support of this linearity is provided by Yu et al. (2005) who observed that the viscous resistance to gas flows through their multi-cavity micro-channels increased linearly with the total number of cavities along the channel. For the validity of the calculations it is further required that the ratio of channel depth to width remains sufficiently small through the later, narrower generations of the 'tree' (so that they qualify as shallow) and that each segment is sufficiently long to ensure that the flow is nearly uniform across its entrance and exit sections. In view of the comments regarding the numerical simulation made at the beginning of Sect. 4 and the results presented in Fig. 3, none of these requirements pose severe restrictions on the applicability of the present procedure. The total resistance of the network thus obtained is

$$R_T = \sum_{k=1}^{M-1} 2^{-k} \left[\frac{2L_k}{D_k}\left(1 + \frac{2\varepsilon\bar{c}}{D_k}\right) + \Delta_0\left(\alpha_{k+1}, \frac{D_k}{2D_{k+1}}\right) + \frac{\varepsilon\bar{c}}{D_{k+1}}\Delta_1\left(\alpha_{k+1}, \frac{D_k}{2D_{k+1}}\right)\right] + 2^{-M}\frac{2L_M}{D_M}\left(1 + \frac{2\varepsilon\bar{c}}{D_M}\right), \tag{29}$$

i.e., the total mass-flow rate through the network is $\dot{m} = \Delta G / R_T$. In Eq. 29 M denotes the total number of generations in the network. For a symmetric network a pair of identical channels branches off from each 'parent' channel. The parameter d appearing in Eq. 22 is here represented by $D_k/2D_{k+1}$ (see Fig. 7b). For the same reason the factor 2^{-k} is preceding the brackets in the summation on the right-hand side of Eq. 29.

In a variety of biological and physiological distribution systems, the variation through the generations of vessel diameters has been observed (Bejan and Lorente 2006; Barber and Emerson 2008) to follow Murray's rule (Murray 1926). For Poiseuille flow through circular cylindrical conduits, this rule is equivalent to requiring a uniform wall shear stress. Requiring instead the uniformity of the mean wall shear stress averaged along the perimeter of the cross section, Barber and Emerson (2008) have recently applied Murray's rule to non-circular cross sections. Since the present calculation is concerned with compressible flow, we require (in light of the above comments) uniformity

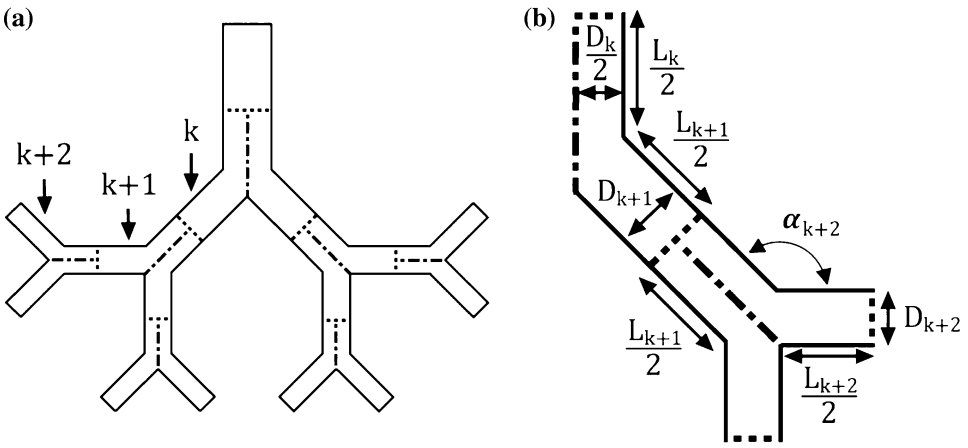

Fig. 7 A schematic description of the generations in a tree-like network (**a**) and the definition of the parameters characterizing successive segments in the network (**b**)

through the geometries of the streamwise gradients of G. This condition allows for the calculation of D_{k+1} for a given D_k, ε and $\bar{c}$. For a network consisting of symmetric bifurcations, we thereby obtain

$$D_{k+1} = \frac{D_k}{2} + \bar{c}\varepsilon \quad k = 1, 2 \ldots M. \tag{30}$$

The above calculation is illustrated in Table 1 which compares at the indicated values of ε the total viscous resistance, R_T, obtained from Eq. 29 for two tree-like networks of rectangular $(\bar{c} \approx 0.63)$ channels. Both networks comprise three generations of symmetric bifurcations ($\alpha = \pi/2$), an equal total network volume and uniform and equal length of branches ($L_k = 2$; all dimensions are normalized by the width of the parent channel of case II). Throughout the network in case I all channels are of the same uniform width, whereas in case II channel widths of successive generations satisfy Eq. 30. According to the table use of Eq. 30 is evidently advantageous.

5 Concluding remarks

We have applied the recently extended Hele-Shaw scheme to study gas flows through shallow micro-channel bends and symmetric bifurcations. The asymptotic scheme effectively reduces the three-dimensional viscous compressible flow problem to a pair of two-dimensional Neumann problems governing the leading order (G_0) and correction (G_1) parts of the quadratic form G. For a given planform configuration these problems need to be solved just *once* (which has been accomplished here by use of conformal mapping yielding analytic solutions for any combination of (α, d)). Subsequently, one readily obtains the complete description for any combination of inlet and outlet conditions, cross-sectional geometry and (sufficiently small) ε. While, in principle there is no difficulty in simulating the flow through each of these configurations, mapping of the entire multidimensional space of parameters characterizing the present problem may become excessively tedious. In view of this, our present scheme provides a useful alternative facilitating a rapid estimate of the performance of these micro-configurations.

Table 1 Comparison of the total viscous resistance of a 3-generation tree with $L_k = 2$, $\alpha_k = 90^0$ (k = 1, 2, 3) and D_k = const. (I) or D_k according to (30) (II)

	Case I	Case II
$\varepsilon = 0.01$	8.56	6.51
$\varepsilon = 0.05$	8.94	6.80
$\varepsilon = 0.1$	9.28	7.04

The present analysis makes use of a continuum slip-flow model to account for weak rarefaction effects. Applicability of these models to small Knudsen number flows through straight and uniform channels have been well established through extensive comparisons with experimental data and DSMC results (cf. Arkilic et al. 1997; Sharipov 1999; Aubert and Colin 2001; Zohar et al. 2002; Ewart et al. 2007 among others). However, in the flow around a sharp edge, local Knudsen numbers may not be small, which warrants some further consideration. A general rule for the applicability of the continuum slip-flow description to non-uniform flows is (cf. Bird 1994; Shen 2005) that the Knudsen number based on local values of both the molecular mean-free path and the macroscopic scale does not exceed ≈ 0.2. The latter scale is commonly defined as the ratio $f/|\nabla f|$ where f generically denotes a representative macroscale quantity. Evidently, in regions of steep gradients this local macroscopic scale may be much smaller than the global characteristic dimension (e.g., the channel depth). Making use of the simulation results (see at the beginning of Sect. 4) for a 90° turn, we have obtained the distribution of the above-defined local Knudsen number throughout the fluid domain. While there is some arbitrariness in the selection of the specific macroscopic

quantity f (e.g., pressure, fluid-speed, and velocity components, etc.,) used to calculate the local macro-scale, the resulting distributions pertaining to the various selections differ only in detail. The local Knudsen numbers exceed 0.2 only within an $O(\varepsilon)$ vicinity of the sharp corner (i.e., within distances comparable with the channel depth). Furthermore, throughout the rest of the configuration, the distribution of local Knudsen number is similar to that obtained in a straight and uniform channel. Thus, the details of the flow in the immediate vicinity of the sharp corner seem to have no global effect. This observation supports our use of the continuum slip-flow model to obtain the mass-flow rate through the shallow configuration.

This conclusion is also supported by the detailed comparison of DSMC results and continuum slip-flow models reported by Beskok (2001) for gas flow over a two-dimensional backward facing step. Beskok has focused on this geometry as a prototype for configurations where steep adverse pressure gradients and flow separation appear as a result of sharp turns. His results show good agreement (including local details of the flow) between the predictions of the continuum model and DSMC results for $Kn \leq 0.1$ (based on channel dimensions, rather than on the more restrictive local microscale defined above). We emphasize that Beskok's study involving high subsonic speeds and a two-dimensional geometry put continuum modeling under a severe test in comparison to the present low-Mach flows through shallow configurations (which effectively suppress the onset of separation; see the discussion in Gat et al. 2008 as well as Yu et al. 2005 and Tsai et al. 2007).

Making use of the linearity of the problem in terms of the quadratic form G (as opposed to the non-linear streamwise pressure variation in compressible flows), we have estimated the total viscous resistance of a tree-like network. Our result incorporating the effects of bifurcations and not just the contribution of the straight channel segments is particularly relevant to 'dense' trees where the lengths of the latter are relatively small. The optimization of such networks on the basis of this result constitutes a useful extension of the present study.

Appendix

For $\alpha = \pi/2$ the transformation (Eq. 20) is explicitly[2]

$$t(\zeta) = \frac{2d}{i\pi}\left\{\tan^{-1}\left(\zeta^{\frac{1}{2}}\right) - \frac{1}{d}\tanh^{-1}\left[\left(d^2\zeta\right)^{\frac{1}{2}}\right]\right\}, \tag{A1}$$

The contributions to Δ (Eq. 25) are

$$\Delta_0 = \frac{1}{\pi}\left(\ln\left(\frac{2+d^2+d^{-2}}{16}\right) + \frac{2}{d}\tan^{-1}(d) + 2d\tan^{-1}\left(d^{-1}\right)\right), \tag{A2}$$

$$\Delta_1 = \frac{2}{\pi}\left(\begin{array}{c}\left(\frac{2}{d^2}+2\right)(1-d)\tan^{-1}(d) + \pi\left(\frac{1}{d}+d\right) \\ +2\left(1-\frac{1}{d}\right)\ln(d) - \frac{\pi}{2}\left(1+\frac{1}{d}\right)\end{array}\right), \tag{A3}$$

for a bend and

$$\Delta_1 = \frac{2}{\pi}\left(\begin{array}{c}\left(-\frac{2}{d}+\frac{1}{d^2}+1-2d\right)\tan^{-1}(d) \\ +\pi\left(\frac{1}{d}+d\right) + \left(2-\frac{1}{d}\right)\ln(d) - \frac{\pi}{2d}\end{array}\right), \tag{A4}$$

for a symmetric bifurcation.

[2] Similar explicit expressions for $\alpha = \pi/4$ and $\alpha = 3\pi/4$ can be obtained directly from the authors.

References

Abramowitz M, Stegun IA (1964) Handbook of mathematical functions. Dover, New York

Agrawal A, Lyazid D, Antonia R (2005) Simulation of gas flow in microchannels with a sudden expansion or contraction. J Fluid Mech 530:135–144

Albertoni S, Cercignani C, Gotusso L (1963) Numerical evaluation of the slip coefficient. Phys Fluids 6:993–996

Alharbi AY, Pence DV, Cullion RN (2003) Fluid flow through microscale fractal-like branching channel networks. J Fluids Eng 125:1051–1057

Arkilic EB, Schmidt MA, Breuer KS (1997) Gaseous slip flow in long microchannels. J Microelectromech Syst 6:167–178

Aubert C, Colin S (2001) High-order boundary conditions for gaseous flows in rectangular microchannels. Microscale Therm Eng 5:41–54

Barber RW, Emerson DR (2008) Optimal design of microfluidic networks using biologically inspired principles. Microfluid Nanofluid 4:179–191

Batchelor G (1967) An introduction to fluid dynamics. Cambridge University press, Cambridge

Bejan A, Lorente S (2006) Constructal theory of generation of configuration in nature and engineering. Appl Phys Rev 100:041301

Beskok A (2001) Validation of a new velocity-slip model for separated gas microflows. Numer Heat Transf Part B 40:451–471

Bird GA (1994) Molecular gas dynamics and the direct simulation of gas flows. Clarendon Press, Oxford

Cercignani C (2000) Rarefied gas dynamics. Macmillan, London

Chen Y, Cheng P (2005) An experimental investigation on the thermal efficiency of fractal tree-like microchannel nets. Int com Heat Mass Transf 32:931–938

Ding X, Yamazaki K (2007) Constructal design of cooling channel in heat transfer system by utilizing optimality of branch systems in nature. J Heat Transf 129:245–255

Durand M (2006) Architecture of optimal transport networks. Phys Rev E 73:016116

Ewart E, Perrier P, Graur IA, Meolans JG (2007) Mass flow rate measurements in a microchannel, from hydrodynamic to near free molecular regimes. J Fluid Mech 584:337–356

Gad-el-Hak M (1999) The fluid mechanics of microdevices. J Fluid Eng 121:5–33

Gad-el-Hak M (2002) The MEMS handbook. CRC press, Boca Raton

Gat AD, Frankel I, Weihs D (2008) Gas flows through constricted shallow micro-channels. J Fluid Mech 602:427–442

Gat AD, Frankel I, Weihs D (2009) A higher-order Hele-Shaw approximation with application to gas flows through shallow micro-channels. J Fluid Mech (in press)

Ghodoossi L (2004) Thermal and hydrodynamical analysis of a fractal microchannel network. Energy convers manag 46:771–788

Ho CM, Tai YC (1996) MEMS and its applications for flow control. J Fluids Eng 118:437–447

Ho CM, Tai YC (1998) Micro-Electro-Mechanical-Systems (MEMS) and fluid flows. Annu Rev Fluid Mech 30:579–612

Lee WY, Wong M, Zohar Y (2001) Gas flow in microchannels with bends. J Micromesh Microeng 11:635–644

Murray C (1926) The physiological principle of minimum work. I. The vacular system and the cost of blood volume. Proc Nat Acad Sci 12:207–214

Polyanin AD (2002) Handbook of linear partial differential equations. Chapman and Hall, London

Senn S, Poulikakos D (2004) Laminar mixing, heat transfer and pressure drop in tree-like microchannel nets and their application for thermal managment in polimer electrolyte fuel cells. J Power Sourc 130:178–191

Sharipov F (1999) Rarefied gas flow through a long rectangular channel. J Vac Sci Technol 17:3062–3066

Shen C (2005) Rarefied gas dynamics: fundamentals, simulations and micro flows. Springer, Berlin

Sone Y (2002) Kinetic theory and fluid dynamics. Brikhauser, Boston

Tsai C-H, Chen H-T, Wang Y-N, Lin C-H, Fu L-M (2007) Capabilities and limitations of 2-dimensional and 3-dimensional numerical methods in modeling the fluid flow in sundden exapansion microchannels. Microfluid Nanofluid 3:13–18

Wechsatol W, Lorente S, Bejan A (2006) Tree-shaped flow structures with local junction losses. Int J Heat Mass Transf 49:2957–2964

White F (1986) Fluid mechanics. McGraw-Hill, New York

Xiong R, Chung J (2007) Flow characteristics of water in straight and serpentine micro-channels with miter bends. Exp Therm Fluid Sci 7:805–812

Yu Z, Lee Y-K, Wong M, Zohar Y (2005) Fluid flows in microchannels with cavities. J Microelectromech Syst 14:1386–1398

Zimaparov V, da Silve A, Bejan A (2006) Thermodynamic optimization of tree-shaped flow geometries with constant channel wall temperature. Int J Heat Mass Transf 49:4839–4849

Zohar Y, Lee SY, Lee WY, Jiang L, Tong P (2002) Subsonic gas flow in a straight and uniform microchannel. J Fluid Mech 472: 125–151